A theory of Snoek relaxation in iron-carbon bct-martensite

Philippe Maugis

A theory of Snoek relaxation in iron-carbon bct-martensite

Philippe Maugis[0000−0001−9283−0471]

Aix Marseille University, CNRS, IM2NP, Marseille, France
philippe.maugis@im2np.fr

Abstract. Martensite is a major constituent of Fe-C alloys. Its metastable body-centered tetragonal structure provides high tensile strength to martensitic steels. Recent experiments highlighted the benefit of large solute carbon content to the strength and ductility of the so-called virgin martensite obtained by sub-zero quench. The results suggest a significant contribution of the elastic and anelastic deformation of the martensite crystals to the rheology of these alloys. In order to shed light on the influence of carbon content on the anelastic response, we investigated theoretically the behavior of solute carbon during Snoek relaxation. Thanks to a linear-response approach, we obtained analytical formulae of the atomic mobilities and the thermodynamic affinities, from which the relaxation strength and time were derived. We unravel the unexpected decrease of the relaxation strength and time when solute carbon content is increased. Relaxation kinetics is explained at the atomic scale by an indirect mechanism of carbon migration in martensite, at variance with ferrite. We emphasize the onset of non-linear effects when the applied stress is high.

Keywords: anelastic behavior · strain relaxation · long-range ordering · mean-field modeling · carbon steels.

1 Introduction

Iron-carbon martensite is the metastable body-centered tetragonal (bct) solid solution of the Fe-C system, wherein carbon atoms are supersaturated in the host lattice. As a microstructural constituent, martensite confers additional hardness to high-strength steels. Plasticity of martensite is well documented [2]. However, the anelastic properties of martensite crystals, i.e. their delayed strain response to an applied stress are less known. These properties are expected to stem from the high amount of carbon soluted in the iron host lattice of martensite. Hence, the stress–strain characteristic of highly carbon-supersaturated "virgin martensite" exhibits high levels of ultimate tensile strength [1], possibly associated to a large anelastic deformation. In the low-carbon ferrite phase, which is also body-centered but cubic, applied stress incites the carbon atoms to redistribute over the interstitial sites. This phenomenon is referred to as Snoek relaxation [31]. It is responsible for delayed deformation and internal friction of low-carbon steels [3]. The relaxation strength in ferrite is proportional to the carbon content is solid solution. Hence, the high amount of carbon soluted in martensite might be expected to provide a high relaxation strength. However, carbon atoms supersaturated in bct-martensite are Zener ordered [37,12,6], i.e. they sit preferentially in one subset of interstitial positions, causing tetragonal distortion of the unit cell. Zener ordering is known to affect carbon migration [8,5,32], which must modify the relaxation time. It may also affect the relaxation strength. The effects of an applied stress on carbon ordering [29,30,15,17] and carbon diffusion [13,19,22] in martensite have been studied theoretically. However, except for the pioneering work of Shtremel in the 70's [27,28], the influence of Zener ordering on the anelastic response of martensite has not been investigated in details so far.

The mechanism of anelasticity in ferrite and martensite involves the alloy thermodynamics of the Fe-C system and the migration properties of the carbon atoms. Previous investigations showed that these properties are controlled by the carbon–strain interaction that arises from the long-range elastic field of the interstitial carbon atoms [15,19]. It results that carbon migration is rendered anisotropic by the Zener ordering [13]: diffusion in directions perpendicular to the axis of tetragonality is accelerated, while parallel diffusion is slowed down [19]. In addition, the response of a martensite crystal to an alternate stress —the internal friction— depends on the direction of the stress: longitudinal or transversal to the axis of tetragonality [9,24]. Furthermore, traction and compression along the tetragonal axis have opposite effects on carbon diffusion [19], from which we expect different relaxation times depending on the sign of the applied stress. Also, the

relaxation time in ferrite is sensitive to the carbon content [18], but the effect in martensite is not known. Furthermore, bct crystals in a martensitic microstructure are subjected to very high internal stresses [7], possibly leading to non-linear effects. In the present study, the above-mentioned effects of Zener order and applied stress have been investigated by means of simulated relaxation experiments where the relaxation time and relaxation strength were retrieved as function of carbon content and stress magnitude.

The thermo-kinetic (TK) model of body-centered Fe-C crystals relies on a mean-field description of the carbon–strain interaction for carbon atoms sitting in stable and in saddle-point position of migration [23]. It describes the time evolution of a carbon-supersaturated solid solution, before segregation to defects and/or precipitation reduces the solute content. It was used in the present study to compute numerically the relaxation kinetics in case of a constant stress applied at time $t = 0$ and then released after the full relaxation is reached. The TK model also served as a starting point for building an analytical theory of Snoek relaxation in martensite crystals, based on the linear-response approximation (LR). Comparison of the LR theory with the TK model highlights the limits of the linear model when high stresses are applied.

2 Model

2.1 The thermo-kinetic model

The thermo-kinetic model (TK) describes the thermodynamics of carbon long-range ordering and the dynamics of carbon migration via a mean-field approximation of the long-range elastic carbon–strain interactions. The model provides the rate equations of the site fractions of carbon on the interstitial sublattices. By means of a first-order development, the linearized rate equations can be obtained (Section 2.2), from which the linear-response approximation is derived (Section 2.3). The TK model is briefly presented in this section, details can be found in Ref. [23].

The material parameters used in our computations are gathered in Table 1. They are described below. This set of parameters provides a good agreement with the Snoek peak measured by Weller in ferrite [35] (see Ref. [23]).

Table 1. Material parameters used in this study: lattice parameter a_0, elastic compliances S_{ij}, force dipole moments P_a and P_c for octahedral (O) and tetrahedral (T) positions, migration enthalpy H_0^m and attempt frequency ν_0.

a_0 (nm)	S_{11} (GPa^{-1})	S_{12} (GPa^{-1})	S_{44} (GPa^{-1})	P_c^O (eV)	P_a^O (eV)	P_c^T (eV)	P_a^T (eV)	H_0^m (eV)	ν_0 (THz)
0.2855	0.00615	−0.00218	0.0104	17.0	10.0	5.37	14.8	0.872	159

In a body-centered iron crystal, solute carbon atoms occupy three types of octahedral interstitial sites, labeled $i = 1, 2, 3$ according to the crystal axis (Figure 1, left). The total carbon fraction C is distributed over the site fractions c_i, such that $C = c_1 + c_2 + c_3$. If the carbon fraction is below the Zener order–disorder transition value, bcc-ferrite is thermodynamically stable, and the three types of sites are equally occupied. Above the transition carbon fraction, one type of site is energetically favored by the carbon–strain interaction (sites labeled 'c'), while the two others are energetically disfavored (sites labeled 'a'). The resulting uneven site occupancy creates a tetragonal distortion of the lattice in direction 1, 2 or 3, depending on the martensite variant Z1, Z2 or Z3. The degree of Zener ordering along crystal direction [001] is be quantified by the structural order parameter $\eta = \left(c_3 - \frac{1}{2}(c_1 + c_2)\right)/C$, while the unequal occupancy of the sites in directions [100] and [010] is quantified by $\zeta = (c_2 - c_1)/C$. In this mean-field description, a variant of martensite is characterized by the couple of values (ζ, η).

To study the relaxation of martensite variants, we considered a pure shear stress tensor applied to the crystal, such that $\sigma_{22} = -\sigma_{11} = \sigma$. Under this stress system, variant Z3 is submitted to a loading 'transversal' to the axis of Zener ordering; Conversely, variants Z1 and Z2 are submitted to a 'longitudinal' loading, where one of the stress components applies in the direction of Zener ordering (Figure 1, right).

Carbon atoms soluted in the octahedral sites of the bcc lattice (labeled $i = 1, 2, 3$) migrate via the saddle-point tetrahedral sites (labeled $j = 1, 2, 3$). In our approach, the interstitial sites are characterized by their force dipole tensor $\boldsymbol{P}^{\mathrm{O}_i}$ or $\boldsymbol{P}^{\mathrm{T}_j}$ characterizing the elastic field induced by a carbon atom in octahedral or

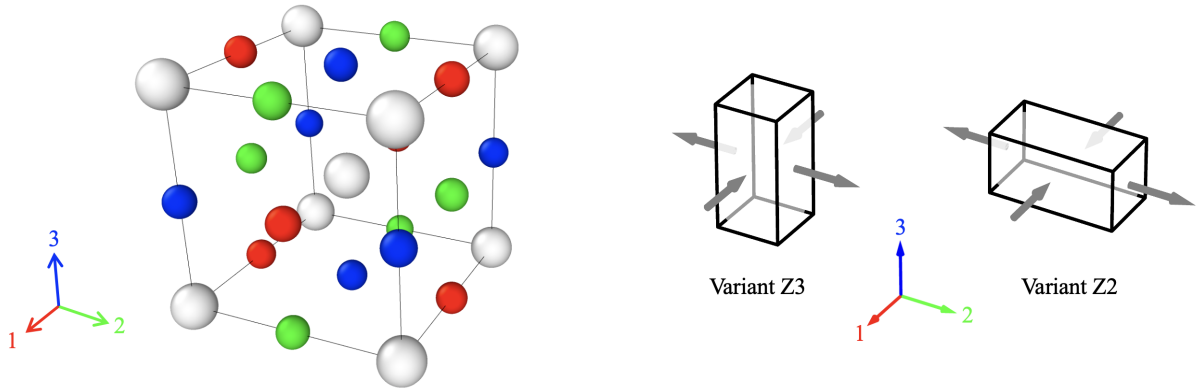

Fig. 1. Left: Crystal cell of body centered iron. Iron atoms are represented by gray spheres, octahedral sites by colored spheres. Sites of type 1, 2, 3 are respectively in color red, green, blue. Right: Schematics of martensite variants Z2 and Z3 submitted to the same shear stress (gray arrows). The loading is said "transversal" for variant Z3, and "longitudinal" for variants Z1 and Z2.

tetrahedral position. Each carbon atom interacts with the homogeneous strain induced by the applied stress and by the other carbon atoms. In the mean-field approximation, this interaction results in the enthalpy function

$$H = -\frac{1}{2} V_0 \boldsymbol{S}(\boldsymbol{\sigma} + \boldsymbol{p}) \cdot (\boldsymbol{\sigma} + \boldsymbol{p}) \tag{1}$$

and the homogeneous strain tensor

$$\boldsymbol{\varepsilon} = \boldsymbol{S}\,(\boldsymbol{\sigma} + \boldsymbol{p})\,. \tag{2}$$

In the above equations, $\boldsymbol{\sigma}$ is the applied stress tensor, $\boldsymbol{p}$ is the force dipole density tensor, $\boldsymbol{S}$ is the elastic compliance tensor of the crystal. The force dipole density tensor is defined as $\boldsymbol{p} = \frac{1}{V_0} \sum c_i \boldsymbol{P}^{\mathrm{O}_i}$, where $V_0 = \frac{1}{2} a_0^3$ is the atomic volume of the lattice. From Equation 2, $\boldsymbol{p}$ can be regarded as the internal stress created by the solute carbon atoms. On account of the high magnitude of tensors $\boldsymbol{P}^{\mathrm{O}_i}$, the internal stress components can reach very high values in martensite: $p_{33} = 2340\,\mathrm{MPa}$ per atom percent of carbon in the direction of tetragonality and $p_{11} = p_{22} = 1380\,\mathrm{MPa/at\%C}$ in the perpendicular direction.

When studying relaxation in crystals, it is usual to introduce the strain dipole tensors $\boldsymbol{\lambda} = \boldsymbol{SP}/V_0$. Due to the tetragonal symmetry of the interstitial sites, these tensors have a singlet component $\lambda_1 = 0.838$ along the tetragonal axis and a doublet component $\lambda_2 = 0.035$ in perpendicular directions. Making use of the strain dipole tensors, the migration enthalpy from site i via the transition site j is written

$$H^{\mathrm{m}}_{i/j} = H^{\mathrm{m}}_0 - V_0 \left(\boldsymbol{\lambda}^{\mathrm{T}_j} - \boldsymbol{\lambda}^{\mathrm{O}_i}\right) \cdot (\boldsymbol{\sigma} + \boldsymbol{p}), \tag{3}$$

where H^{m}_0 is the migration enthalpy in the stress-free carbon-free crystal. We see from this equation that both the applied stress and the carbon distribution contribute to modifying the migration enthalpy. According to the rate theory in the mean-field approximation, the jump frequency is written, in the dilute approximation: $\Gamma_{i/j} = \nu_0\, c_i \exp\left(-H^{\mathrm{m}}_{i/j}/k_{\mathrm{B}}T\right)$. The net flux from i to k is $J_{i\to k} = \Gamma_{i/j} - \Gamma_{k/j}$. Then the matter balance at site i implies the rate equations

$$\frac{\mathrm{d}c_i}{\mathrm{d}t} = 2\,(J_{k\to i} + J_{k'\to i})\,, \quad i = 1, 2, 3. \tag{4}$$

2.2 Linearized rate equations

Starting from the rate equations (Eqs. 4) we look for linearized equations relating the rate of change of the order parameters ζ and η to the corresponding affinities A_ζ and A_η. The first step of the calculation is to establish the non-linear equations that express the flux as a product of a driving force by an atomic mobility. Then the equations are linearized in an Onsager-like form. Introducing the affinities and applying the matter balance produces the linearized rate equations.

We first notice that the flux $J_{i\to k}$ between sites i and k, as defined in Section 2.1, is a difference in the form $p-q$. Then, following Martin [14], we use Polkowicz's identity $p-q=\sqrt{pq}\left(\sqrt{p/q}-\sqrt{q/p}\right)$ to write the flux as a product of the driving force

$$k_{\mathrm{B}}T\sqrt{\frac{p}{q}-\frac{q}{p}}=2k_{\mathrm{B}}T\sinh\frac{\mu_i-\mu_k}{2k_{\mathrm{B}}T} \tag{5}$$

and the atomic mobility

$$\frac{\sqrt{pq}}{k_{\mathrm{B}}T}=M_{ik}. \tag{6}$$

Function $\mu_i=\partial G/\partial c_i$ is the chemical potential of sites i. Equation 5 shows that the flux between sites i and k results form the bias in chemical potential $\mu_i-\mu_k$. At equilibrium, all fluxes vanish, i.e. $J_{1\to 2}=J_{2\to 3}=J_{3\to 1}=0$, which, according to Equation 5 implies the equality of the chemical potentials: $\mu_1=\mu_2=\mu_3$. Hence, the flux equations of our model are compatible with the model's thermodynamics. This ensures that a relaxing system will converge towards the proper thermodynamic equilibrium.

Let us assume that the system remains close to the equilibrium state. Under this condition the flux $J_{i\to k}$ linearizes into an Onsager-type of equation:

$$J_{i\to k}=M_{ik}\left(\mu_i-\mu_k\right), \tag{7}$$

i.e. the flux between two types of sites is proportional to the difference in chemical potential between the sites. The intensity of the flux depends on the magnitude of the mobility M_{ik}. From Equation 6 the mobility expands into

$$M_{ik}=\frac{\nu_0\sqrt{c_ic_k}}{k_{\mathrm{B}}T}\exp\left(-\frac{H_0^{\mathrm{m}}+V_0\Delta\boldsymbol{\lambda}^{ik}\cdot(\boldsymbol{\sigma}+\boldsymbol{p})}{k_{\mathrm{B}}T}\right). \tag{8}$$

$\Delta\boldsymbol{\lambda}^{ik}$ is a symmetric rank-2 tensor, function of the elastic properties of stable sites i and k, and transition site j:

$$\Delta\boldsymbol{\lambda}^{ik}=-\boldsymbol{\lambda}^{\mathrm{T}_j}+\frac{\boldsymbol{\lambda}^{\mathrm{O}_i}+\boldsymbol{\lambda}^{\mathrm{O}_k}}{2}. \tag{9}$$

The second term in the exponential of Equation 8 expresses the effect of both the applied stress (via $\boldsymbol{\sigma}$) and the carbon atom distribution (via $\boldsymbol{p}$) on the activation energy of the atomic mobility. The site fractions c_i entering the expression of M_{ik} in the square root and in the dipole density $\boldsymbol{p}$ are the equilibrium values under stress $\boldsymbol{\sigma}$. Site fractions c_i and c_k in the pre-exponential factor represent the amount of carbon atoms susceptible to participate to matter exchange between sites i and k.

Following Nowick and Berry [25], we establish the kinetic equations of relaxation. Introducing the Onsager relationship (Eq. 7) into the set of rate equations (Eqs. 4) yields the differential equations of the order parameters:

$$\begin{cases}\dfrac{\mathrm{d}\zeta}{dt}=\dfrac{2}{C^2}\left(\left(4M_{12}+M_{13}+M_{23}\right)A_\zeta+\dfrac{3}{2}\left(M_{13}-M_{23}\right)A_\eta\right)\\[2ex] \dfrac{\mathrm{d}\eta}{dt}=\dfrac{3}{C^2}\left(\left(M_{13}-M_{23}\right)A_\zeta+\dfrac{3}{2}\left(M_{13}+M_{23}\right)A_\eta\right)\end{cases} \tag{10}$$

These equations are linear in the affinities $A_\zeta=-\partial G/\partial\zeta$ and $A_\eta=-\partial G/\partial\eta$ related to parameters ζ and η respectively. Deviation from zero of the affinities appears as the driving force for the time evolution of the order parameters. Such a deviation can be induced by an applied stress in a relaxation experiment. The resulting relaxation kinetics will depend on the values of the three independent mobilities M_{12}, M_{13} and M_{23}. The relaxed state $\dot\zeta=\dot\eta=0$ is reached when the affinities both equal zero, which defines thermodynamic equilibrium. Here, a singularity of martensite as compared to ferrite resides in the relaxation of *two* order parameters in martensite rather than a unique parameter in ferrite [18].

2.3 The linear-response approximation

When the system is close to stress-free thermodynamic equilibrium, an analytical solution to the kinetic equations (Eqs. 10) can be found by linearizing the affinities with respect to the order parameters ζ, η and to

the shear stress σ. This approach was used to investigate the giant Snoek peak in disordered Fe-C ferrite by linearizing around the equilibrium disordered state [18]. Conversely to ferrite, linearization in martensite has to be performed in the vicinity of the *ordered* equilibrium state. An analytical expression of the equilibrium order parameters is then required.

Using the enthalpy function H (Eq. 1) and the regular entropy S in the dilute approximation, the Gibbs energy $G = H - TS$ is written as function of the external variables C, T, σ and the internal variables ζ, η [18]. Performing partial derivation with respect to ζ and η yields the expression of the affinities:

$$\begin{cases} A_\zeta = \dfrac{3}{2} h_\Sigma C^2 \zeta + V_\Sigma C \sigma - \dfrac{1}{2} k_\mathrm{B} T C \ln\left(\dfrac{1 + \frac{3}{2}\zeta - \eta}{1 - \frac{3}{2}\zeta - \eta}\right) \\ A_\eta = 2 h_\Sigma C^2 \eta - \dfrac{1}{3} k_\mathrm{B} T C \ln\left(\dfrac{(1+2\eta)^2}{\left(1 + \frac{3}{2}\zeta - \eta\right)\left(1 - \frac{3}{2}\zeta - \eta\right)}\right) \end{cases} \tag{11}$$

Notice that, thanks to a proper choice of the order parameters, the effect of applied stress σ on the affinities is carried by A_ζ alone. In these equations, we introduced the strain-energy parameter

$$h_\Sigma = \frac{2 V_0 (\lambda_1 - \lambda_2)^2}{3 S'} \tag{12}$$

and the strain-stress parameter

$$V_\Sigma = V_0 (\lambda_1 - \lambda_2). \tag{13}$$

These parameters characterize respectively the magnitude of the carbon–carbon and carbon–stress elastic interactions in the mean-field approximation. $S' = 2(S_{11} - S_{12})$ is the shear compliance. Numerically, $h_\Sigma = 1.87\,\mathrm{eV}$ and $V_\Sigma = 0.803\,V_0$.

When no stress is applied, the system undergoes an order–disorder transition at carbon content $C_0 = \left(\frac{4}{3}\ln 2\right) k_\mathrm{B} T / h_\Sigma$ [15]. If carbon content is lower than C_0, the unique solution to the equilibrium equations is $\zeta = \eta = 0$, which corresponds to disordered ferrite. If carbon content is higher than C_0, three pairs of degenerate solutions (ζ, η) correspond to the three ordered orientational variants of martensite. Variant Z3, for instance, bears a tetragonal axis along crystal direction 3, and its equilibrium order parameters write $\zeta = 0$ and $\eta = \eta_0$. Function $\eta_0(C)$ is presented in Figure 2, where the carbon content C^* is expressed in units of $k_\mathrm{B} T / h_\Sigma$. The order–disorder transition occurs at $C_0^* \simeq 0.924$. The ordering curves of variants Z1 and Z2 are defined by $\zeta = -\eta_0$ and $\zeta = \eta_0$ respectively, and $\eta = -\frac{1}{2}\zeta$.

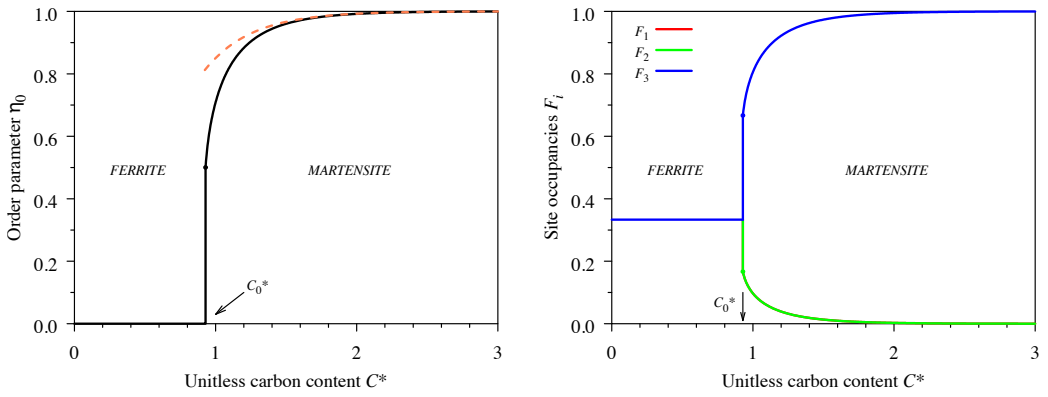

Fig. 2. Left: longitudinal order parameter as function of unitless carbon content. The dashed line is the high-carbon approximation (Eq. 14). Right: equilibrium site occupancies $F_i = c_i/C$ in variant Z3. The ferrite–martensite ordering transition occurs at unitless carbon content $C_0^* \simeq 0.924$. When carbon content increases in martensite, the favored sites (site-3) enrich in carbon at the expense of the disfavored ones (site-1 and 2).

When the carbon content is much higher than C_0, the equilibrium order parameter η_0 is close to 1: the favored sites contain the large majority of carbon atoms, while the disfavored sites are almost carbon-

depleted, as shown in Figure 2, right. In this case, the equilibrium order parameter can approximated by the formula

$$\eta_0 \simeq 1 - 3\exp\left(-\frac{3h_\Sigma C}{k_\mathrm{B}T}\right), \tag{14}$$

where $H' = 3h_\Sigma C$ expresses the difference in site energy between favored and disfavored sites.

In order to get rate equations linearized in stress, the mobilities are evaluated at $\boldsymbol{\sigma} = \mathbf{0}$. Then, on account of the crystal symmetry, the number of independent mobilities reduces to two: M_ac is the mobility between disfavored sites (type a) and favored sites (type c), while M_aa is the mobility between two disfavored sites. For instance, in variant Z3 the favored sites are of type 3, and we have $M_\mathrm{ac} = M_{13} = M_{23}$ and $M_\mathrm{aa} = M_{12}$. From Equation 8 applied to the equilibrium site fractions c_i, we find the zeroth-order expression of the mobilities:

$$\begin{cases} M_\mathrm{ac} = \dfrac{\nu_0 C}{k_\mathrm{B}T}\exp\left(-\dfrac{H_0^\mathrm{m}}{k_\mathrm{B}T}\right)\exp\left(-\dfrac{\Delta\boldsymbol{\lambda}^{13}\cdot\boldsymbol{P}^{\mathrm{O}_3}C + \frac{3}{2}h_\Sigma C}{k_\mathrm{B}T}\right) \\ M_\mathrm{aa} = \dfrac{\nu_0 C}{k_\mathrm{B}T}\exp\left(-\dfrac{H_0^\mathrm{m}}{k_\mathrm{B}T}\right)\exp\left(-\dfrac{\Delta\boldsymbol{\lambda}^{12}\cdot\boldsymbol{P}^{\mathrm{O}_3}C + 3h_\Sigma C}{k_\mathrm{B}T}\right) \end{cases} \tag{15}$$

In these expressions, the mobilities M_ac and M_aa between pairs of sites differ by two carbon-dependent terms in the activation enthalpy: 1) The term containing the strain-energy parameter h_Σ accounts for the difference in energy between favored and disfavored sites. Each disfavored site of the pair contributes by $\frac{3}{2}h_\Sigma C$ to the activation enthalpy. Consequently, the contribution to M_aa is twice the contribution to M_ac; 2) The term $\Delta\boldsymbol{\lambda}\cdot\boldsymbol{P}C$ renders the effect of the tetragonal distortion of the crystal on the saddle-point energy for migration. This effect depends on the direction of the jump (perpendicular $a \leftrightarrow c$ or parallel $a \leftrightarrow a$ to the tetragonality axis).

On account of the tetragonal symmetry of bct-martensite, the anelastic response of the crystal depends on the orientation of the stress relative to the axis of Zener order. We considered the transversal loading with variant Z3, and the longitudinal loading with variant Z2 (see Figure 1, right). In the longitudinal case, one component of the stress tensor applies along the tetragonality axis, thus modifying Zener ordering. Hence, we expect a higher relaxation strength in the longitudinal case than in the transversal case.

Case of transversal loading We consider variant Z3 submitted to as transversal shear stress. The applied stress induces deviations of the order parameters from the stress-free situation, noted $\Delta\zeta(\sigma) = \zeta$ and $\Delta\eta = \eta(\sigma) - \eta_0$. Using the approximation of Equation 14, a first-order development in $\Delta\zeta$ and $\Delta\eta$ gives the linearized affinities as functions of ζ, $\Delta\eta$, C, T and σ:

$$\begin{cases} A_\zeta = -\dfrac{1}{2}A_0 C\zeta + V_\Sigma C\sigma \\ A_\eta = -\dfrac{2}{9}A_0 C\Delta\eta \end{cases} \tag{16}$$

Function A_0 is defined as

$$A_0(C,T) = k_\mathrm{B}T\exp\left(\frac{3h_\Sigma C}{k_\mathrm{B}T}\right). \tag{17}$$

The exponential factor in A_0 originates from the C and T dependency of the equilibrium order parameters of tetragonal martensite (Eq. 14).

Equations 16 are decoupled, such that the equilibrium value of $\Delta\eta$ is not affected by the applied stress. Then, to the first order, η remains constantly equal to its stress-free equilibrium value during relaxation: the relaxed value $\Delta\eta_R = 0$ and the affinity $A_\eta = 0$ at all times. The applied stress only affects the order parameter ζ, i.e. relaxation occurs by carbon exchanges between sites 1 and 2, not involving the carbon atoms located in sites 3. From the condition $A_\zeta = 0$ and using the definitions of A_0 and V_Σ we find the relaxed value of ζ:

$$\zeta_\mathrm{R} = 2\frac{V_0(\lambda_1 - \lambda_2)}{k_\mathrm{B}T}\exp\left(-\frac{3h_\Sigma C}{k_\mathrm{B}T}\right)\sigma. \tag{18}$$

We see that ζ_R in martensite differs by an exponential factor from its expression in ferrite [25,18]: $\zeta_\mathrm{R} = \zeta_\mathrm{R}^\mathrm{ferr} \times 3\exp(-3h_\Sigma C/k_\mathrm{B}T)$. On account of this exponential factor, the relaxed value in martensite *decreases*

when the carbon content in solution is increased. The reason for this surprising behavior is as follows: contrary to ferrite, in variant Z3 under transversal loading, only the carbon atoms located in sites 1 and 2 contribute to the anelastic response. The proportion of these atoms is precisely $(c_1 + c_2)/C = 3\exp(-3h_\Sigma C/k_\mathrm{B}T)$. When the carbon content is increased, this proportion decreases in relation with the increased Zener order (see Figure 2). As a consequence, the relaxed order parameter ζ_R decreases.

Making use of the relaxed value ζ_R (Eq. 18), the affinities are simply written as function of the deviation form the relaxed state:

$$\begin{cases} A_\zeta = -\dfrac{1}{2}A_0 C\,(\zeta - \zeta_R) \\ A_\eta = 0 \end{cases} \tag{19}$$

Following an equivalent approach to Nowick and Berry [25], we look for the relaxation of the strain when a constant stress is applied or suppressed at time $t = 0$. From the time dependency of the strain, the time relaxation τ and the relaxation strength Δ can be extracted. Introducing the affinities of Equation 19 into the linearized rate equations 10, we find the relaxation equation of ζ:

$$\frac{\mathrm{d}\zeta}{\mathrm{d}t} = -\frac{2}{C}(2M_\mathrm{aa} + M_\mathrm{ac})A_0(\zeta - \zeta_R). \tag{20}$$

From the stress–strain relationship (Eq. 2), the shear strain, defined as reference to stress-free martensite, is

$$\varepsilon = S'\sigma + \frac{V_\Sigma C}{V_0}\zeta. \tag{21}$$

The first term in the right-hand side is the elastic response ε_U while the second term is the anelastic response ε^an. Solving Equation 20 and using Equation 21, we find

$$\frac{\varepsilon^\mathrm{an}(t)}{\varepsilon_\mathrm{U}} = \Delta^\mathrm{trans}\exp\left(-\frac{t}{\tau^\mathrm{trans}}\right) \tag{22}$$

in case of relaxation after suppressing a stress at time $t = 0$, and

$$\frac{\varepsilon^\mathrm{an}(t)}{\varepsilon_\mathrm{U}} = \Delta^\mathrm{trans}\left[1 - \exp\left(-\frac{t}{\tau^\mathrm{trans}}\right)\right] \tag{23}$$

in case of relaxation after applying a stress at $t = 0$. The relaxation strength Δ^trans quantifies the magnitude of the anelastic relaxation. In our linear-response approximation, it is stress-independent, and is expressed as

$$\Delta^\mathrm{trans} = \left(\frac{3h_\Sigma C}{k_\mathrm{B}T}\right)\exp\left(-\frac{3h_\Sigma C}{k_\mathrm{B}T}\right). \tag{24}$$

Compared to ferrite [18], the relaxation strength in martensite is reduced by the factor $3\exp(-3h_\Sigma C/k_\mathrm{B}T)$, on account of the depletion of the disfavored sites to the benefit of the favored sites. The higher the solute carbon content of martensite, the lower is the magnitude of the relaxation strength.

From the relaxation Equation 20, we see that the relaxation time is related to mobilities M_aa and M_ac. It combines two characteristic times:

$$\frac{1}{\tau^\mathrm{trans}} = \frac{1}{\tau_\mathrm{ac}} + \frac{1}{\tau_\mathrm{aa}}. \tag{25}$$

τ_ac is proportional to the reciprocal mobility M_ac^{-1}. It is characteristic of the carbon exchanges between favored and disfavored sites. τ_aa, proportional to the reciprocal mobility M_aa^{-1}, is characteristic of the carbon exchanges between the disfavored sites. These two mechanisms contribute in parallel to the atom transfer between sites 1 and sites 2 when a shear stress is applied. The characteristic times are expressed as:

$$\begin{cases} \dfrac{1}{\tau_\mathrm{ac}} = 2\nu_0\exp\left(-\dfrac{H_0^\mathrm{m} + \Delta H_\mathrm{ac}C}{k_\mathrm{B}T}\right) \\ \dfrac{1}{\tau_\mathrm{aa}} = 4\nu_0\exp\left(-\dfrac{H_0^\mathrm{m} + \Delta H_\mathrm{aa}C}{k_\mathrm{B}T}\right) \end{cases} \tag{26}$$

They are carbon-content dependent via the activation enthalpies:

$$\begin{cases} \Delta H_{\mathrm{ac}} = \Delta\boldsymbol{\lambda}^{13} \cdot \boldsymbol{P}^{\mathrm{O}_3} - \dfrac{3}{2} h_\Sigma \\ \Delta H_{\mathrm{aa}} = \Delta\boldsymbol{\lambda}^{12} \cdot \boldsymbol{P}^{\mathrm{O}_3} \end{cases} \tag{27}$$

The numerical values of $\Delta H_{\mathrm{ac}} = -3.79\,\mathrm{eV}$ and $\Delta H_{\mathrm{aa}} = 3.78\,\mathrm{eV}$ show that the disfavored-favored exchanges are accelerated by the carbon–strain interaction, while the disfavored-disfavored ones are slowed down. At room temperature Equation 26 implies $\tau_{\mathrm{aa}} \gg \tau_{\mathrm{ac}}$. Hence, according to the additivity rule of Equation 25, the kinetics of relaxation is controlled by the fastest mechanism —the $a \leftrightarrow c$ exchanges—, and the relaxation time is approximately $\tau^{\mathrm{trans}} \simeq \tau_{\mathrm{ac}}$.

Case of longitudinal loading We now consider variant Z2, whose tetragonal axis is in line with component σ_{22} of the stress tensor (see Figure 1, right). At stress-free equilibrium the order parameters are $\zeta = \eta_0(C,T)$ and $\eta = -\frac{1}{2}\eta_0(C,T)$. An applied shear stress modifies the Zener order of this variant by inducing a net flux of atoms between favored and disfavored sites. It also modifies the balance between the disfavored sites 1 and 3, because direction 1 is stressed ($\sigma_{11} \neq 0$) while direction 3 is not ($\sigma_{33} = 0$). The resulting deviations of order parameters from stress-free equilibrium are noted $\Delta\zeta = \zeta(\sigma) - \eta_0$ and $\Delta\eta = \eta(\sigma) + \frac{1}{2}\eta_0$. Using the approximation of Equation 14, the linearized affinities are written:

$$\begin{cases} A_\zeta = -\dfrac{1}{4} A_0 C(\Delta\zeta - \Delta\zeta_{\mathrm{R}}) - \dfrac{1}{6} A_0 C(\Delta\eta - \Delta\eta_{\mathrm{R}}) \\ A_\eta = -\dfrac{1}{6} A_0 C(\Delta\zeta - \Delta\zeta_{\mathrm{R}}) - \dfrac{5}{9} A_0 C(\Delta\eta - \Delta\eta_{\mathrm{R}}) \end{cases} \tag{28}$$

with the relaxed values:

$$\begin{cases} \Delta\zeta_{\mathrm{R}} = 5\dfrac{V_0(\lambda_1 - \lambda_2)}{k_{\mathrm{B}}T} \exp\left(-\dfrac{3h_\Sigma C}{k_{\mathrm{B}}T}\right)\sigma \\ \Delta\eta_{\mathrm{R}} = -\dfrac{3}{2}\dfrac{V_0(\lambda_1 - \lambda_2)}{k_{\mathrm{B}}T} \exp\left(-\dfrac{3h_\Sigma C}{k_{\mathrm{B}}T}\right)\sigma \end{cases} \tag{29}$$

Contrary to the transversal case, the affinities are coupled in the longitudinal case, i.e. both A_ζ and A_η functions depend on the deviations from stressed equilibrium expressed by $\Delta\zeta - \Delta\zeta_{\mathrm{R}}$ and $\Delta\eta - \Delta\eta_{\mathrm{R}}$. As a consequence, the rate equations of $\Delta\zeta$ and $\Delta\eta$ are coupled:

$$\begin{cases} \dfrac{\mathrm{d}\Delta\zeta}{\mathrm{d}t} = -\left(\dfrac{1}{\tau_{\mathrm{ac}}} + \dfrac{1}{4\tau_{\mathrm{aa}}}\right)(\Delta\zeta - \Delta\zeta_{\mathrm{R}}) - \dfrac{1}{2\tau_{\mathrm{aa}}}(\Delta\eta - \Delta\eta_{\mathrm{R}}) \\ \dfrac{\mathrm{d}\Delta\eta}{\mathrm{d}t} = -\dfrac{3}{8\tau_{\mathrm{aa}}}(\Delta\zeta - \Delta\zeta_{\mathrm{R}}) - \left(\dfrac{1}{\tau_{\mathrm{ac}}} + \dfrac{3}{4\tau_{\mathrm{aa}}}\right)(\Delta\eta - \Delta\eta_{\mathrm{R}}) \end{cases} \tag{30}$$

This system of linear differential equations admits two eigen states ($\parallel$ and $\perp$), related to the following eigen values:

$$\begin{cases} \dfrac{1}{\tau_\parallel} = \dfrac{1}{\tau_{\mathrm{ac}}} \\ \dfrac{1}{\tau_\perp} = \dfrac{1}{\tau_{\mathrm{ac}}} + \dfrac{1}{\tau_{\mathrm{aa}}} \end{cases} \tag{31}$$

Eigen value $1/\tau_\parallel$ is associated to the order parameter $\eta' = \frac{3}{4}(\zeta - \frac{2}{3}\eta)$, which quantifies Zener order along direction 2: $\eta' = \left(c_2 - \frac{1}{2}(c_1 + c_3)\right)/C$. Eigen value $1/\tau_\perp$ is associated to the order parameter $\zeta' = \frac{1}{2}(\zeta + 2\eta) = (c_3 - c_1)/C$, which quantifies the degree of orthorhombicity, or "beyond Zener" ordering [17]. Notice that $\tau_\perp$ identifies with the relaxation time under transversal loading τ^{trans} (Eq. 25). Numerically, the relaxation times $\tau_\parallel$ and $\tau_\perp$ are very close to one another since $\tau_{\mathrm{aa}} \gg \tau_{\mathrm{ac}}$, as discussed above. The corresponding eigen states $\parallel$ and $\perp$ represent respectively parallel and perpendicular modes of relaxation relative to the crystal direction of the Zener ordering. The solution to Equations 30 in case of relaxation from stressed equilibrium is

$$\begin{cases} \Delta\zeta(t) = \Delta\zeta_{\mathrm{R}}\left[\dfrac{9}{10}\exp\left(-\dfrac{t}{\tau_\parallel}\right) + \dfrac{1}{10}\exp\left(-\dfrac{t}{\tau_\perp}\right)\right] \\ \Delta\eta(t) = \Delta\eta_{\mathrm{R}}\left[\dfrac{3}{2}\exp\left(-\dfrac{t}{\tau_\parallel}\right) - \dfrac{1}{2}\exp\left(-\dfrac{t}{\tau_\perp}\right)\right] \end{cases} \tag{32}$$

Using the expression of the strain Equation 21, we find the time evolution of the anelastic strain:

$$\frac{\varepsilon^{\mathrm{an}}(t)}{\varepsilon_{\mathrm{U}}} = \Delta_{\parallel} \exp\left(-\frac{t}{\tau_{\parallel}}\right) + \Delta_{\perp} \exp\left(-\frac{t}{\tau_{\perp}}\right), \tag{33}$$

with the relaxation strengths of the $\parallel$ and $\perp$ modes:

$$\begin{cases} \Delta_{\parallel} = \dfrac{9}{4}\left(\dfrac{3h_{\Sigma}C}{k_{\mathrm{B}}T}\right)\exp\left(-\dfrac{3h_{\Sigma}C}{k_{\mathrm{B}}T}\right) \\ \Delta_{\perp} = \dfrac{1}{4}\left(\dfrac{3h_{\Sigma}C}{k_{\mathrm{B}}T}\right)\exp\left(-\dfrac{3h_{\Sigma}C}{k_{\mathrm{B}}T}\right) \end{cases} \tag{34}$$

We see that the relaxation strength of the parallel mode ($\Delta_{\parallel}$) is 9 times higher than that of the perpendicular mode ($\Delta_{\perp}$): as expected, relaxation of the Zener ordering provides most of the relaxation strength. Similarly to the transversal case, the relaxation strengths in the longitudinal case decrease exponentially with the carbon content.

2.4 The single-relaxation approximation

We recall that the characteristic times are very different in magnitude, such that $\tau_{\mathrm{aa}} \gg \tau_{\mathrm{ac}}$. In the single-relaxation approximation, we neglect τ_{aa}^{-1} as regards to τ_{ac}^{-1} in the expressions of the relaxation times (Eqs. 25 and 31). Under this approximation, all relaxation times are equal and have the same carbon-content dependency:

$$\tau^{(\mathrm{SR})} = (2\nu_0)^{-1} \exp\left(\frac{H_0^{\mathrm{m}} + \Delta H_{\mathrm{ac}} C}{k_{\mathrm{B}}T}\right). \tag{35}$$

From Equations 24 and 34, the total longitudinal strength $\Delta_{\parallel} + \Delta_{\perp}$ is written

$$\Delta^{\mathrm{longi(SR)}} = \frac{5}{2}\left(\frac{3h_{\Sigma}C}{k_{\mathrm{B}}T}\right)\exp\left(-\frac{3h_{\Sigma}C}{k_{\mathrm{B}}T}\right). \tag{36}$$

In the single-relaxation approximation, transversal and longitudinal responses share the same relaxation time, but longitudinal relaxation $\Delta^{\mathrm{longi(SR)}}$ is 2.5 times stronger than transversal relaxation Δ^{trans} (Eq. 24).

3 Results

3.1 Numerical test

Our thermo-kinetic model (TK) describes the relaxation kinetics of body-centered Fe-C by a set of mean-field rate equations (Eq. 4). These equations are non-linear in the order parameters and in the applied stress. When linearized, the rate equations give rise to the linear-response approximation (LR) of the relaxation kinetics of martensite, from which the relaxation time and strength under transversal and longitudinal shear stress were derived (Eqs. 24, 25, 31 and 34). The linear-response approximation is a priori valid in the vicinity of thermodynamic equilibrium, i.e. for low applied stress. In order to test the limits of the LR approximation, we compared its predictions with the TK model for various stress magnitudes. Figure 3 presents the relaxation kinetics of the 3 at% C alloy at 300 K under shear stress of 1, 10 and 100 MPa. Time evolution of the anelastic strain $\varepsilon_{\mathrm{an}}$ scaled by the elastic strain ε_{U} has a typical shape: the relaxation time is defined as the time interval after which the strain amplitude has increased by a factor of $1 - e^{-1} \simeq 63.2\%$; the relaxation strength is the asymptotic value. In the case of transversal loading, we see that the relaxation kinetics is insensitive to the magnitude of the stress. As a consequence, the LR model is a good approximation of the relaxation kinetics. In the case of longitudinal loading however, the relaxation time and strength appear to depend on the magnitude of the stress, and the agreement between LR and TK models is poorer.

A second limit to the linear-response approximation is that is it restricted to carbon content large enough compared to the transition value C_0. At temperature $T = 300\,\mathrm{K}$ the transition occurs when $C_0 = 1.28\,\mathrm{at\%}$. The next sections investigate the effect of carbon content and stress magnitude on the relaxation kinetics and compare the TK and LR predictions.

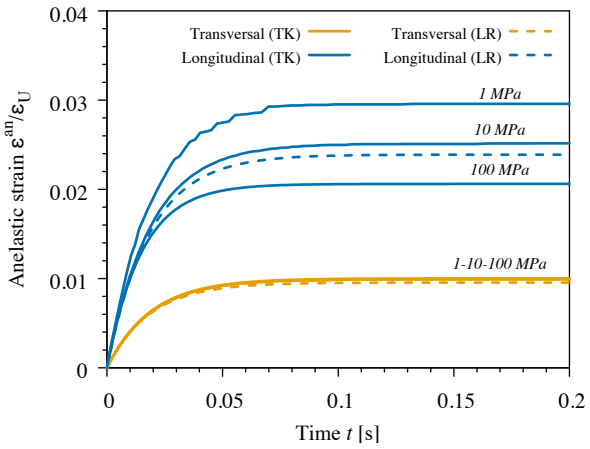

Fig. 3. Comparison between the thermo-kinetic model (TK) and the linear response approximation (LR) for various applied stress, under transversal or longitudinal loading. The carbon content is set to $C = 3\,\text{at}\%$.

3.2 Kinetics of relaxation: effect of carbon content

Relaxation kinetics computed with the TK model for various carbon contents and an applied stress of 100 MPa are gathered in Figure 4. As expected from the linear approximation, relaxation is about 2.5 times higher in case of longitudinal loading compared to transversal loading. In both cases, the relaxed strain *decreases* when the carbon content is increased, as does the relaxation time.

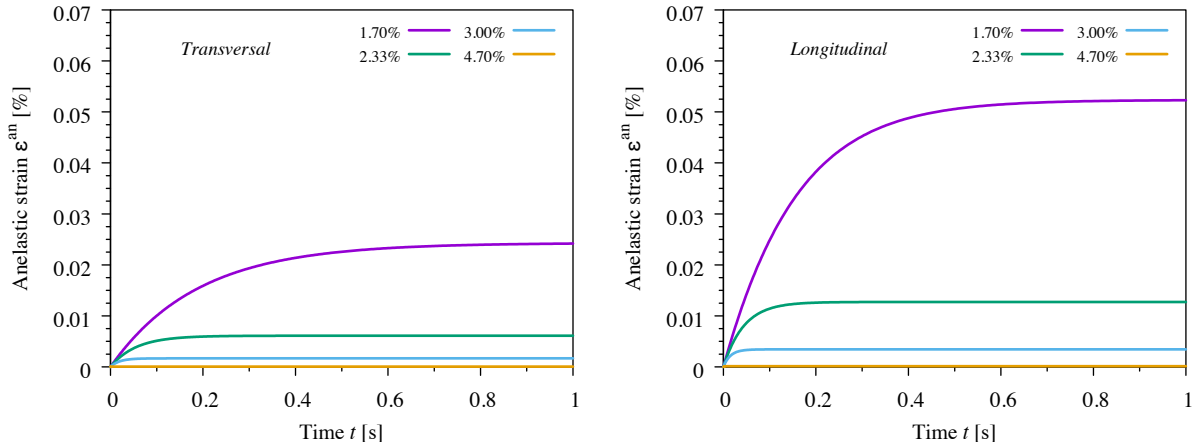

Fig. 4. Effect of carbon content on the kinetics of relaxation computed at $T = 300\,\text{K}$ under shear stress $\sigma = 100\,\text{MPa}$ with the thermo-kinetic model. Transversal (left) and longitudinal (right) loading.

The effect of carbon content is summarized in Figure 5. We see that both the relaxation strength and relaxation time decrease when the carbon content is increased. This fact is in accordance with the linear-response approximation (circles in Figure 5). The agreement between TK and LR models is very good for the transversal case, at least when the carbon content is higher than $\sim 3\,\text{at}\%$. A discrepancy is visible in the longitudinal case, related to the influence of stress magnitude on relaxation.

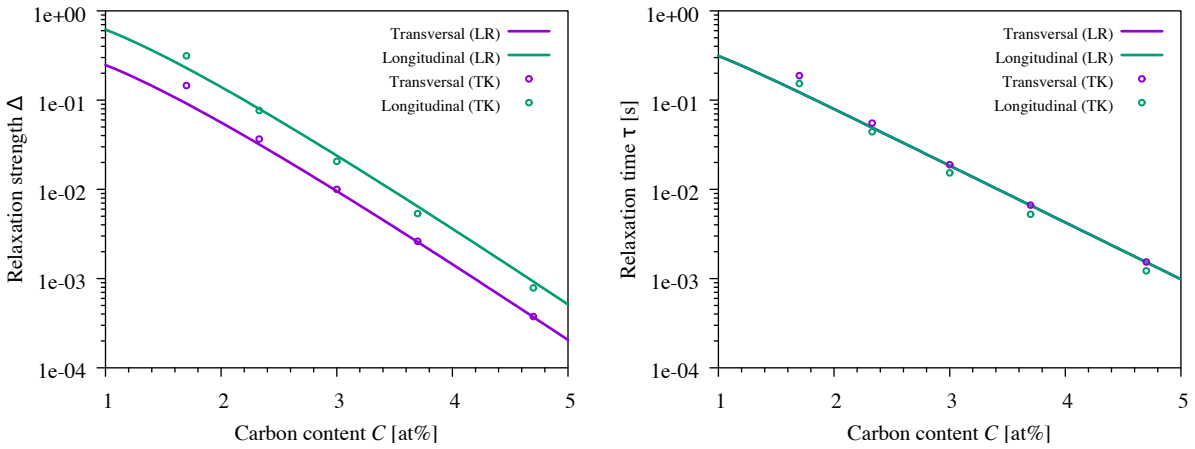

Fig. 5. Effect of carbon content on the relaxation strength (left) and relaxation time (right) computed at $T = 300\,\mathrm{K}$ under shear stress $\sigma = 100\,\mathrm{MPa}$. Comparison between the thermo-kinetic model (TK) and the linear-response approximation (LR). The discrepancy at high carbon content evidences the non-linear effect of longitudinal stress.

3.3 Kinetics of relaxation: effect of stress magnitude

Section 3.1 evidenced that the relaxation time depends on the magnitude of the applied stress. Under this circumstance, we must distinguish two types of relaxation: (1) loading, where a stress is applied during relaxation; and (2) unloading, where no stress is applied during relaxation. Indeed, during loading the applied stress modifies carbon mobilities according to Equation 8, hence modifying the relaxation time compared to unloading. Figure 6 gathers a series of relaxation kinetics during loading followed by unloading, under various applied stress. We checked that the response to a transversal solicitation is proportional to the applied stress, such that the relaxation strength is not affected by the magnitude of the stress, whether positive or negative. In addition, the relaxation time is also stress-independent. On the other hand, for a longitudinal solicitation, the stress–strain relationship is not linear: the higher the stress, the lower is the relaxation strength (see Figure 7, left). The relaxation time also varies with the applied stress. Its stress-sensitivity depends on the type of relaxation: it decreases by a factor of ~ 10 between -100 MPa and 500 MPa in the case of loading and by a smaller factor in the case of unloading (see Figure 7, right).

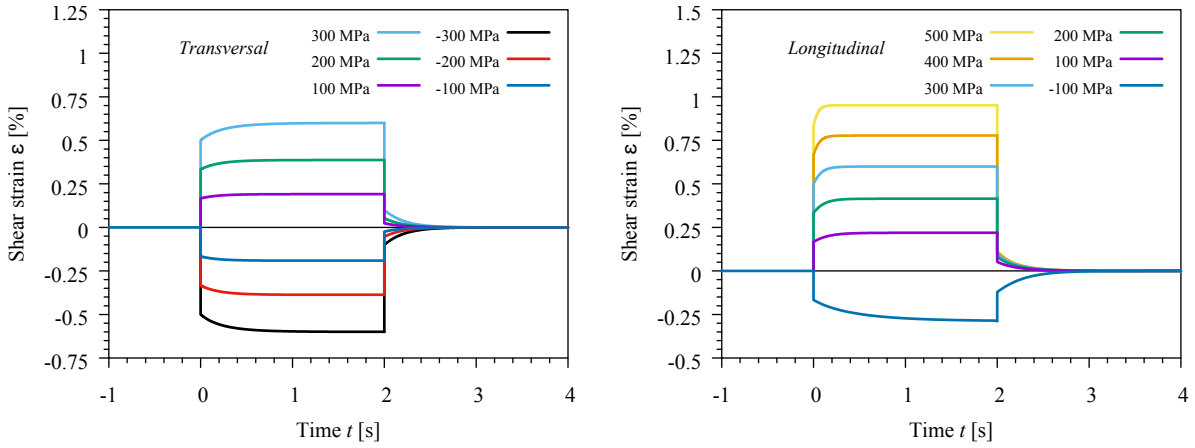

Fig. 6. Time evolution of the total shear strain during loading and unloading under various applied stress, at $T = 300\,\mathrm{K}$ and carbon content $C = 1.7\,\mathrm{at\%}$. In case of longitudinal solicitation (right figure), the relaxation time decreases when the stress is increased.

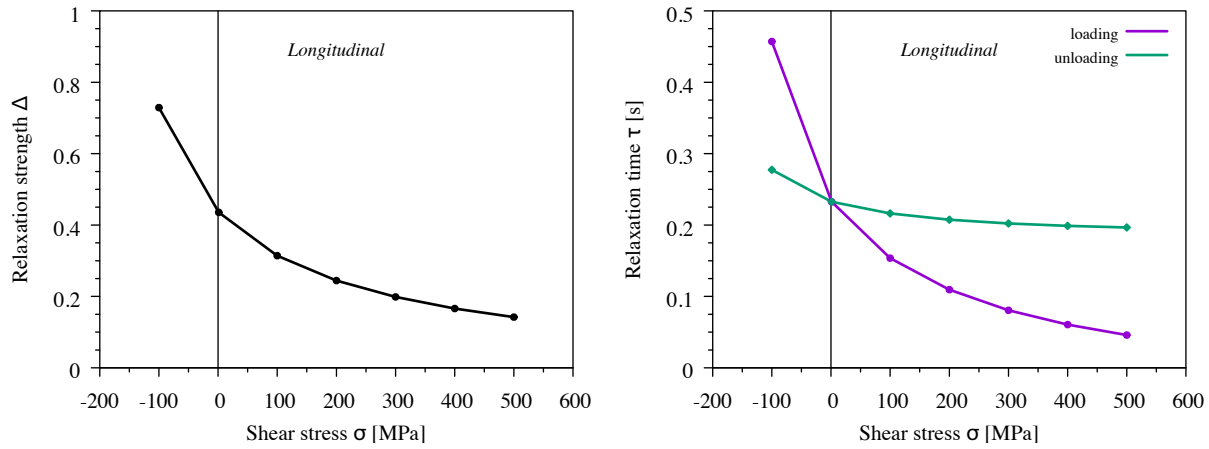

Fig. 7. Effect of longitudinal stress on the relaxation strength (left) and relaxation time (right) computed by the thermo-kinetic model at $T = 300\,\mathrm{K}$ and carbon content $C = 1.7\,\mathrm{at}\%$.

4 Discussion

4.1 Influence of short-range carbon–carbon interactions

From Section 2.3, we see that the relaxation strengths in martensite depend on the key parameter h_Σ, which characterizes carbon–carbon interactions in bcc-iron. The accuracy of our predictions relies on the accuracy of h_Σ.

Parameter h_Σ corresponds to the strain-energy parameter $\lambda_0 = 3h_\Sigma$, as defined by Khachaturyan in relation to the order–disorder transition temperature $T_0 = 0.361\,\lambda_0 C/k_\mathrm{B}$ [21,11]. Our value $\lambda_0 = 5.62$ eV was derived from ab initio calculations of the force dipole tensor of carbon and of the elastic stiffness coefficients of bcc iron. It is informative to compare this value with the literature. Recent studies used various computational and experimental techniques from which λ_0 could be extracted. The techniques fall into three categories: (i) direct computation of pair interactions by embedded atom potential (EAM) [34] or density functional theory (DFT) [33,26]; (ii) indirect evaluation from molecular dynamics simulations [29,4]; and (iii) indirect evaluation from x-ray diffraction data (XRD) [36]. The values are gathered in Table 2. They are very scattered, and range from 3.15 to 10.8 eV. Our value of 5.62 eV lies in the middle of the range.

Table 2. Strain-interaction parameter λ_0 (in eV). Comparison with literature.

Ref.	Technique	λ_0 (eV)
This work	DFT	5.62
Udyansky et al. [34]	EAM	10.8
Udyansky et al. [33]	DFT	6.34
Ruban [26]	DFT	9.5
Sinclair et al. [29]	EAM	3.15
Chirkov et al. [4]	EAM	5.55
Xiao et al. [36]	XRD	8.53

A more meaningful comparison can be obtained from the tetragonality parameter $\lambda_1 - \lambda_2$, which quantifies the carbon-induced strain field. In fact, $(\lambda_1 - \lambda_2)^2$ is proportional to the magnitude of the Snoek relaxation. Now, the internal friction profile predicted in ferrite from our value $\lambda_1 - \lambda_2 = 0.803$ is close to the experimental profile within 10% [18,23]. We may conclude that our prediction of the Snoek relaxation in martensite is also within these 10% of accuracy. However, the short-range carbon–carbon interactions are not taken into

account in the present study, although they are expected to have a larger influence in high-carbon martensite than in low-carbon ferrite. They may thus modify the relaxation strength of martensite.

Kinetic Monte Carlo simulations allowed to investigate the effect of carbon–carbon short-range interactions on the relaxation of martensite. Actually, internal friction profiles computed by Huang et al. [9] show that short-range interactions have almost no influence on the Snoek peak of martensite, except for a minor additional peak at temperature $\sim 330\,\mathrm{K}$. From this, we conclude that short-range interactions can be neglected, as a first approach, in the present study of Snoek relaxation.

The present theory applies to a single crystal of martensite containing a unique orientational variant. Elaboration of such a crystal is out of reach nowadays, so direct confrontation with experiment is not feasible. However, indirect verification may be achieved with polycrystals: this would necessitate prior measure of the sample texture, and modeling the polycrystal response via the Reuss averaging method [25,10].

4.2 Origins of non-linear relaxation

In case of transversal solicitation, we have seen that the relaxation kinetics is insensitive to the magnitude of the stress. This is because transversal stress has little effect on Zener ordering. As a consequence, the LR model is a good approximation of the relaxation kinetics under transversal loading/unloading. In case of longitudinal loading/unloading however, the relaxation time and strengths depend on stress because longitudinal stress affects the Zener order, thus modifying both the site occupancies and the migration barriers.

The linear-response approximation can be used to understand the effect of stress on mobility. When a stress is applied, both the equilibrium site fractions and the activation enthalpies are modified. This affects the mobility via two factors (see Equation 8): (i) the pre-exponential factor $\sqrt{c_i c_k}$, which varies with time during relaxation; and (ii) the activation enthalpy, which is affected by both the stress $\boldsymbol{\sigma}$ and the time variations in dipole density $\boldsymbol{p}$. In case of transversal loading/unloading, these effects cancel out for symmetry reasons, such that the relaxation time τ^{trans} does not depend on stress magnitude, at least to the first order. In case of longitudinal loading/unloading, the components of the stress tensor act both along the tetragonality axis and perpendicular to it. Their effects on the equilibrium site fractions and on the activation enthalpies differ, resulting in a net change in the relaxation time τ^{longi}. In addition, because of the change in site fractions induced by the stress, the mobility is no longer time-independent under high applied stress.

The effect of stress on the relaxation strength results from the non-linearity of the affinity A_ζ as function of order parameter ζ (Eq. 11), from which the relationship between the relaxed strain and the stress is non linear. Figure 8 presents stress–strain curves computed under very low stress rate ($< 1\,\mathrm{MPa/s}$), such that the system remains close to equilibrium along the test. We see that the mechanical compliance increases when carbon content is reduced. The compliance is higher in the longitudinal case than in the transversal case, in relation to the higher longitudinal relaxation strength. Non-linearity of the stress–strain relationship is apparent at carbon content of $1.70\,\mathrm{at\%}$. Notice that in the longitudinal case, positive and negative shear stress produce non symmetrical effects: martensite is more compliant under negative shear stress (i.e. when compression is applied along the tetragonal axis) than under positive shear stress (i.e. when tension is applied along the tetragonal axis). This is coherent with the tensile/compressive stress–strain relationship computed by kinetic Monte Carlo simulations [16].

4.3 Link with carbon diffusivity

It has been reported that carbon diffusivity in bct-martensite is slower than in bcc-ferrite [5,20]. Hillert suggested that Zener ordering of the carbon atoms in martensite increases the activation barrier for their migration, thus limiting long-range diffusion [8]. This idea was partly confirmed by molecular dynamic simulations of Perez et al. [29] and by Monte Carlo simulations of Maugis et al. [19]: the simulations showed that some of the activation barriers are indeed increased by the Zener order, such that long-range diffusion is slowed down when the carbon content increases. However, one of the activation barriers is *decreased* when the carbon content is increased, providing easy migration paths. As the relaxation mechanism involves short-range diffusion rather than long-range diffusion, one may expect that the "easy jumps" accelerate Snoek relaxation in martensite, as compared to ferrite. This point is discussed below.

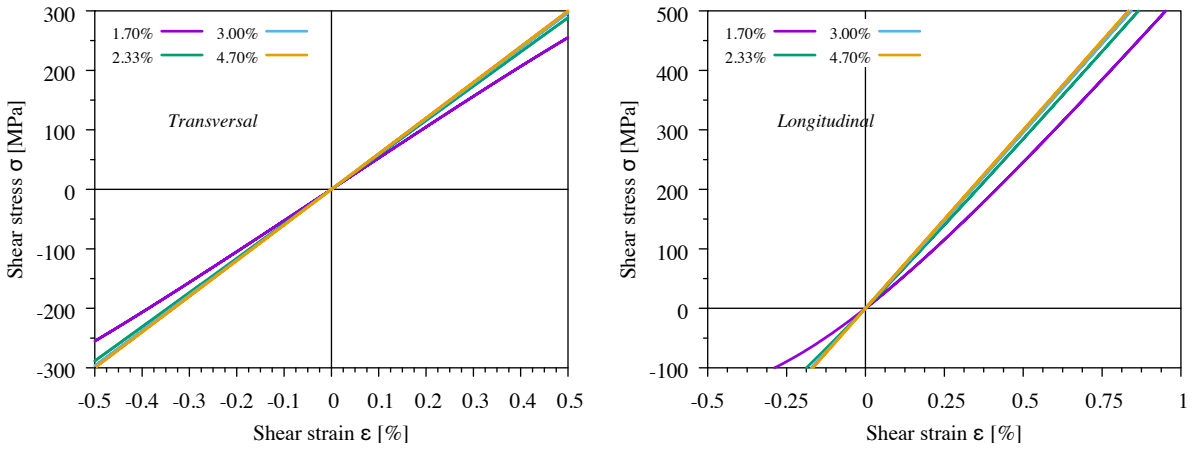

Fig. 8. Shear mechanical test computed at $T = 300\,\mathrm{K}$ for various carbon contents. The stress rate is kept lower than 1 MPa/s. Reducing the carbon content in martensite increases the compliance and induces a non-linear response.

In ferrite, the activation enthalpy of the relaxation time τ identifies with the migration barrier of carbon, noted $H_0^{\mathrm{m}} = 0.872\,\mathrm{eV}$. At variance, tetragonal martensite has two activation enthalpies for relaxation, related to the characteristic times τ_{aa} and τ_{ac} (see Section 2.3). The enthalpies are linearly dependent on carbon fraction C (unitless): a high $H_{\mathrm{aa}} = 0.872 + 3.78\,C$ for disfavored–disfavored ($a \leftrightarrow a$) exchanges, and a low $H_{\mathrm{ac}} = 0.872 - 3.79\,C$ for disfavored–favored ($a \leftrightarrow c$) exchanges. These activation enthalpies can be linked to the migration barriers of carbon in martensite, as shown in the following.

Carbon migration in martensite was investigated by means of the elasto-chemical model by Maugis et al. [19]. It was found that carbon–strain interaction splits the migration barrier H_0^{m} into three different values: $H_{a\to a} = 0.872 + 3.77\,C$ for parallel jumps; $H_{a\to c} = 0.872 - 3.81\,C$ and $H_{c\to a} = 0.872 + 1.82\,C$ for perpendicular jumps (see Figure 9). The migration barriers are not independent. In particular, the barrier $H_{c\to a}$ for jumping out of a favored site is higher than the barrier $H_{a\to c}$ for jumping into a favored site, by the quantity $H' = 3h_\Sigma C$. H' is the difference in site energy that favors sites c compared to sites a. Comparing the analytical formulae of Ref. [19] with the present study (Eq. 27) yields the simple —although not intuitive— identification: $H_{\mathrm{aa}} = H_{a\to a}$ and $H_{\mathrm{ac}} = H_{a\to c}$. Thus, the relatively slow $a \leftrightarrow a$ exchanges are controlled by the migration barrier of the $a \to a$ jumps, whereas the $a \leftrightarrow c$ exchanges are relatively fast thanks to the easy $a \to c$ jumps.

Section 2.4 reported that relaxation kinetics is controlled by the shortest characteristic time, τ_{ac}. Thus the activation enthalpy for relaxation is H_{ac}, which corresponds to carbon migration perpendicular to the axis of tetragonality. Notice that, although H_{ac} identifies with the activation barrier of the fast $a \to c$ jump, the relaxation mechanism also involves the slower $c \to a$ jump. Further, in the case of perpendicular loading/unloading, relaxation occurs via forward $a_1 \to c \to a_2$ and backward $a_2 \to c \to a_1$ chains of jumps, among which $a \to c$ is fast while $c \to a$ is slow (see Figure 10). This indirect mechanism proves to be more efficient that the direct mechanism $a_1 \to a_2$ and $a_2 \to a_1$ of carbon migration parallel to the tetragonality axis.

Finally, as the enthalpy H_{ac} decreases when the carbon content is increased, relaxation is faster when the carbon content is high. This important result is not contradictory with slower diffusivity when increasing the carbon content: in effect, relaxation is related to short-range diffusion, involving the low $H_{a\to c}$ barrier, which decreases when the carbon content is increased. Conversely, long-range diffusion involves a combination of migration barriers, that decreases diffusivity when the carbon content is increased [19].

5 Conclusion

To study the strain relaxation in bct-martensite, we adopted a mean-field approximation of carbon migration in the iron host lattice deformed by the strain field of carbon atoms. By linearizing the kinetic equations in

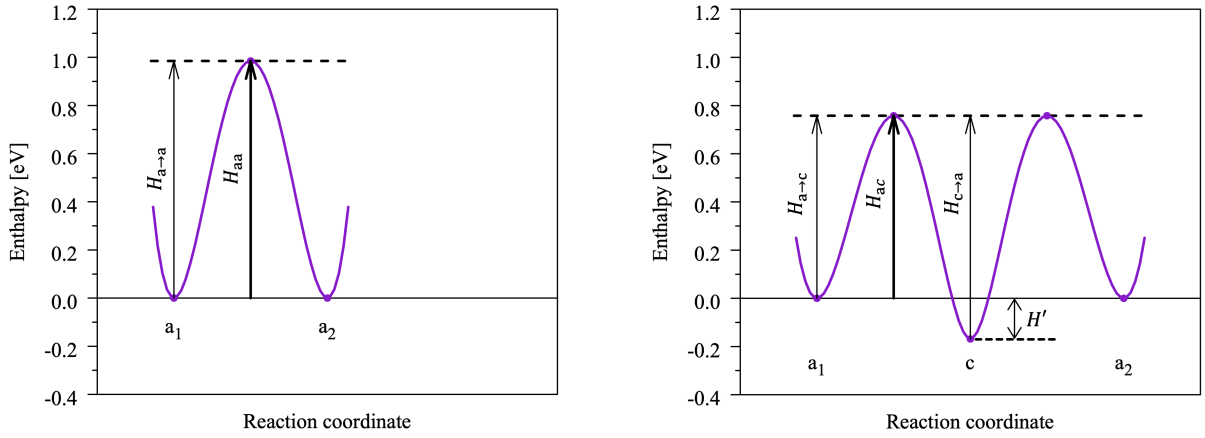

Fig. 9. Energy paths during relaxation by carbon exchange between disfavored sites: direct path $a_1 \to a_2$ (left) and indirect path $a_1 \to c \to a_2$ (right). Relaxation by the indirect path via favored site c has a lower activation enthalpy ($H_{ac} = 0.76\,\text{eV}$) than by the direct path ($H_{aa} = 0.99\,\text{eV}$). The carbon content was set to $C = 3\,\text{at}\%$. The lines are polynomial interpolations between calculated points.

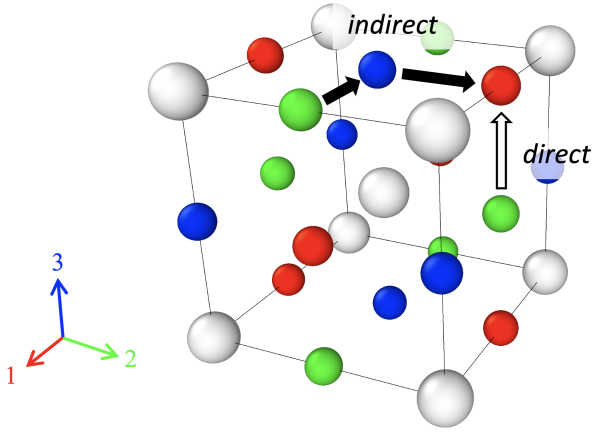

Fig. 10. Direct and indirect pathways for carbon exchange between two disfavored sites (red and green spheres) of variant Z3. The indirect mechanism, across a transitory favored site (blue sphere), is faster than the direct one.

the vicinity of thermodynamic equilibrium, we built the linear response theory of Snoek relaxation in bct-martensite. The model involves atomic mobilities and thermodynamic affinities, from which the influence of carbon content on Snoek relaxation could be derived. Our results exhibit the major role of Zener ordering, which reduces the relaxation strength compared to ferrite, and also reduces the relaxation time. The main conclusions of our study are the following:

- When linearized, the kinetic equations for relaxation bring up two thermally activated atomic mobilities, which are connected to two characteristic times. One characteristic time is related to direct carbon exchanges between disfavored interstitial sites, which are relatively slow; the other characteristic time is related to exchanges between favored and disfavored sites, which are relatively fast.
- Two directions of shear loading/unloading with respect to crystal orientation were distinguished: transversal when the stress components are perpendicular to the tetragonality axis; longitudinal when one stress component is along the tetragonality axis. Both cases share approximately the same relaxation time, but the strength of longitudinal relaxation is 2.5 times the strength of transversal relaxation.
- Analysis of the relaxation times reveals that relaxation in case of transversal loading involves an indirect mechanism of carbon migration: to perform matter exchange between disfavored sites, carbon atoms

transit via the favored sites. This provides faster relaxation that direct exchange between disfavored sites.
– When increasing the applied stress, two sources of non-linearity appear: 1) non-linearity of the atomic mobility, which produces a stress-dependent relaxation time; and 2) non-linearity of the thermodynamic affinities, which causes a non-linear stress–strain relationship.

These results are a first step to understanding the influence of the stress rate on the mechanical response of martensite crystals.

Declaration of Competing Interest

The authors declare that they have no known competing financial interests or personal relationships that could have appeared to influence the work reported in this paper.

Acknowledgments

This work was supported by the Agence Nationale de la Recherche, France (contract C-TRAM ANR-18-CE92-0021). The paper is dedicated to Georges Martin, who introduced the invaluable Polkowicz's identity in the mean-field kinetic theory of alloys.

References

1. Allain, S., Danoix, F., Goune, M., Hummada, K., Mangelinck, D.: Static and dynamical ageing processes at room temperature in a Fe25Ni0.4C virgin martensite: Effect of C redistribution at the nanoscale. Philos. Mag. Lett. **93**(2), 68–76 (2013). https://doi.org/10.1080/09500839.2012.742590
2. Bhadeshia, H.K.D.H., Honeycombe, R.W.K.: Steels: microstructure and properties. Metallurgy and materials science series, E. Arnold, London New York, 3rd ed. edn. (2006)
3. Blanter, M., Golovin, I., Neuhauser, H., Sinning, H.R.: Internal Friction in Metallic Materials. Springer-Verlag, Berlin Heidelberg, 1st edn. (2007)
4. Chirkov, P., Mirzoev, A., Mirzaev, D.: Molecular-dynamics Simulations of Carbon Ordering in bcc Fe and its Impact on Martensite Transition. Mater. Today Proc. **2S**, 553–556 (jan 2015). https://doi.org/10.1016/J.MATPR.2015.07.345, http://www.sciencedirect.com/science/article/pii/S2214785315005908
5. DeCristofaro, N., Kaplow, R., Owen, W.S.: The kinetics of carbon clustering in martensite. Metall. Trans. A **9**, 821–825 (1978)
6. Epp, J., Hirsch, T., Curfs, C.: In situ X-Ray Diffraction Analysis of Carbon Partitioning During Quenching of Low Carbon Steel. Metall. Mater. Trans. A **43**(7), 2210–2217 (2012)
7. Genderen, M.J., Isac, M., Böttger, A., Mittemeijer, E.J.: Aging and tempering behavior of iron-nickel-carbon and iron-carbon martensite. Metall. Mater. Trans. A **28**(March), 545–561 (1997). https://doi.org/10.1007/s11661-997-0042-5
8. Hillert, M.: The kinetics of the first stage of tempering. Acta Metall. **7**(10), 653–658 (1959)
9. Huang, L., Maugis, P.: Effect of substitutional Ni atoms on the Snoek relaxation in ferrite and martensite Fe-C alloys : An atomisitic investigation. Comput. Mater. Sci. **203**, 111083 (2022). https://doi.org/10.1016/j.commatsci.2021.111083, https://doi.org/10.1016/j.commatsci.2021.111083
10. Ino, H., Takagi, S., Sugeno, T.: On the relaxation strength of the Snoek peak. Acta Metall. **15**, 29–34 (1967)
11. Kurdjumov, G., Khachaturyan, A.: Phenomena of carbon atom redistribution in martensite. Metall. Trans. **3**(5), 1069–1076 (1972). https://doi.org/10.1007/BF02642438
12. Kurdjumov, G., Khachaturyan, A.: Nature of axial ratio anomalies of the martensite lattice and mechanism of diffusionless gamma to alpha transformation. Acta Metall. **23**, 1077–1088 (1975)
13. Lawrence, B., Sinclair, C.W., Perez, M.: Carbon diffusion in supersaturated ferrite : A comparison of mean-field and atomistic predictions. Model. Simul. Mater. Sci. Eng. **22**, 1–17 (2014). https://doi.org/10.1088/0965-0393/22/6/065003
14. Martin, G.: Atomic mobility in Cahn's diffusion model. Phys. Rev. B **41**(4), 2279–2283 (1990). https://doi.org/10.1103/PhysRevB.41.2279
15. Maugis, P.: Ferrite, martensite and supercritical iron: A coherent elastochemical theory of stress-induced carbon ordering in steel. Acta Mater. **158**, 454–465 (2018)

16. Maugis, P.: Nonlinear elastic behavior of iron-carbon alloys at the nanoscale. Comput. Mater. Sci. **159**, 460–469 (2019)
17. Maugis, P.: A Temperature–Stress Phase Diagram of Carbon-Supersaturated bcc-Iron, Exhibiting "Beyond-Zener" Ordering. J. Phase Equilibria Diffus. **41**, 269–275 (may 2020). https://doi.org/10.1007/s11669-020-00816-2
18. Maugis, P.: Giant Snoek peak in ferrite due to carbon-carbon strain interactions. Materialia **12**(8), 100805 (2020). https://doi.org/10.1016/j.mtla.2020.100805
19. Maugis, P., Chentouf, S., Connétable, D.: Stress-controlled carbon diffusion channeling in bct-iron: A mean-field theory. J. Alloys Compd. **769**, 1121–1131 (2018)
20. Maugis, P., Danoix, F., Dumont, M., Curelea, S., Cazottes, S., Zapolsky, H., Gouné, M.: Carbon diffusivity and kinetics of spinodal decomposition of martensite in a model Fe-Ni-C alloy. Mater. Lett. **214**, 213–216 (2018). https://doi.org/10.1016/j.matlet.2017.12.007
21. Maugis, P., Danoix, F., Zapolsky, H., Cazottes, S., Gouné, M.: Temperature hysteresis of the order-disorder transition in carbon-supersaturated α-Fe. Phys. Rev. B **96**(21), 214104 (2017)
22. Maugis, P., Kandaskalov, D.: Revisiting the pressure effect on Carbon migration in iron. Mater. Lett. **270**, 127725 (mar 2020). https://doi.org/10.1016/J.MATLET.2020.127725
23. Maugis, P.: Thermo-kinetic modelling of the giant Snoek effect in carbon-supersaturated iron. J. Alloys Compd. **877**, 160236 (may 2021)
24. Maugis, P., Huang, L.: Modeling the Snoek peak in bct-martensite. J. Alloys Compd. **907**, 164502 (jun 2022). https://doi.org/10.1016/J.JALLCOM.2022.164502, https://linkinghub.elsevier.com/retrieve/pii/S0925838822008933
25. Nowick, A.S., Berry, B.: Anelastic relaxation in crystalline solids. Materials science series, Academic Press, New York (1972)
26. Ruban, A.V.: Self-trapping of carbon atoms in alpha'-Fe during the martensitic transformation: A qualitative picture from ab initio calculations. Phys. Rev. B - Condens. Matter Mater. Phys. **90**(14), 144106 (2014)
27. Shtremel, M., Satdarova, F.: Ordering kinetics of interstitial solid solutions. Sov. Phys. - Solid State **13**(4), 835–840 (1971)
28. Shtremel, M., Satdarova, F.: Influence of stresses on order in interstitial solutions. Fiz. Met. Met. **34**(4), 699–708 (1972)
29. Sinclair, C.W., Perez, M., Veiga, R.G.A., Weck, A.: Molecular dynamics study of the ordering of carbon in highly supersaturated alpha-Fe. Phys. Rev. B **81**(22), 224204 (2010)
30. Sinclair, C.W., Perez, M.: Ordering in Highly Supersaturated Alpha-Fe-C. Solid State Phenom. **172-174**, 996–1001 (2011)
31. Snoek, J.: Effect of small quantities of carbon and nitrogen on the elastic and plastic properties of iron. Physica **8**(7), 711–733 (1941). https://doi.org/10.1016/S0031-8914(41)90517-7
32. Taylor, K., Cohen, M.: Ageing of ferrous martensites. Prog. Mater. Sci. **36**, 225–272 (1992)
33. Udyansky, A., von Pezold, J., Dick, A., Neugebauer, J.: Orientational ordering of interstitial atoms and martensite formation in dilute Fe-based solid solutions. Phys. Rev. B **83**(18), 184112 (2011)
34. Udyansky, A., Von Pezold, J., Bugaev, V.N., Friák, M., Neugebauer, J.: Interplay between long-range elastic and short-range chemical interactions in Fe-C martensite formation. Phys. Rev. B - Condens. Matter Mater. Phys. **79**(22), 224112 (2009)
35. Weller, M.: The Snoek relaxation in bcc metals-From steel wire to meteorites. Mater. Sci. Eng. A **442**(1-2 SPEC. ISS.), 21–30 (2006). https://doi.org/10.1016/j.msea.2006.02.232
36. Xiao, L., Fan, Z., Jinxiu, Z., Mingxing, Z., Mokuang, K., Zhenqi, G.: Lattice-parameter variation with carbon content of martensite. I. X-ray-diffraction experimental study. Phys. Rev. B **52**(14), 9970–9978 (1995)
37. Zener, C.: Theory of strain interaction of solute atoms. Phys. Rev. **74**(6), 639–647 (1948). https://doi.org/10.1103/PhysRev.74.639